Hindawi
Mathematical Problems in Engineering
Volume 2023, Article ID 7970139, 14 pages
https://doi.org/10.1155/2023/7970139

Research Article

Dynamic Analysis of Marine Drilling Risers Considering Steady Current, Surface Wave, Internal Solitary Wave, and Vessel Motion

Guanghai Gao,[1] **Yulong Li**,[2] **Xiao Cong**,[3] **Kunshan Xu**,[1] **and Yunjing Cui**[4]

[1]*College of Chemistry & Chemical Engineering, Yantai University, Yantai 264005, China*
[2]*Liaodong Operation Company of CNOOC (China) Co. Ltd., Tianjin Branch LD6–2CEPA, Tianjin 330451, China*
[3]*Shandong Special Equipment Inspection Institute Co. Ltd., Jinan 250101, China*
[4]*College of Mechanical and Electronic Engineering, China University of Petroleum (East China), Qingdao 266580, China*

Correspondence should be addressed to Guanghai Gao; ggh8912@126.com

Received 28 March 2023; Revised 22 July 2023; Accepted 24 August 2023; Published 20 September 2023

Academic Editor: Francesco Aymerich

In this paper, considering combined excitations of the steady current, surface wave, internal solitary wave as well as, the vessel's surge and heave motions, a time-domain model is established to investigate the lateral dynamic response of marine drilling risers. The finite element and Newmark-β methods are used to solve the nonlinear partial differential equation in the time-domain. The entire numerical solution process is realized by a self-developed program based on MATLAB. The reliability of the numerical solution program is verified by comparing it with published numerical results. The lateral dynamic responses of a real-scale marine drilling riser, usually used in the deep water oil/gas industry in the South China Sea, are studied. The impact level of each factor in the riser's lateral dynamic response is discussed.

1. Introduction

Marine drilling risers play a significant role in the oil/gas industry in the South China Sea. Complex environmental conditions can greatly threaten the risers' safe operation. The internal solitary wave (ISW) is one of these complex influential factors. So far, many researchers have studied the main features of the ISW in the South China Sea [1, 2]. At present, Korteweg-de Vries (KdV), mKdV, and Miyata-Choi-Camassa theoretical models are mainly used to simulate ISW [3, 4]. On the basis of these theoretical models, some researchers have studied the loads induced by the ISWs on small-scale cylinders or marine slender structures. The modified Morrison formula is usually adopted to calculate the forces induced by ISW. Cai et al. [5, 6] and Xie et al. [7] researched the loads on cylindrical piles. Si et al. [8] studied the shear forces and torques induced by a large amplitude ISW on a rigid pile. Xu et al. [9] investigated the forces induced by the depression and elevation of ISWs on cylindrical piles. Zha et al. [10] studied the force acting on cylindrical piles based on the observations and in situ buoyancy frequency data deriving from nautical X-band radar. Some researchers have also conducted experimental investigations on the forces induced by ISW on submerged small-scale cylinders [11–13]. In addition, some researchers have studied the forces induced by ISWs on other types of marine structures [14–16]. Comparisons of the effects of surface waves and ISWs on marine structures have also been conducted by some researchers [17, 18].

Vessel's motion is another an important influential factor in the dynamic analysis of marine drilling risers. Sexton and Agbezuge [19] studied the effects of surface random waves, steady currents and vessel's surge motions on the dynamic response of marine drilling risers. Park and Jung [20] analyzed the dynamic response of marine structures while considering the combined excitations of the vessel's heave motion and force. Guo et al. [21] studied the dynamic response of a top tensioned riser considering the combined excitations of the surface wave, ISW and vessel's surge motion. Adamiec-Wójcik et al. [22] adopted the rigid finite element method to study the dynamic response of marine

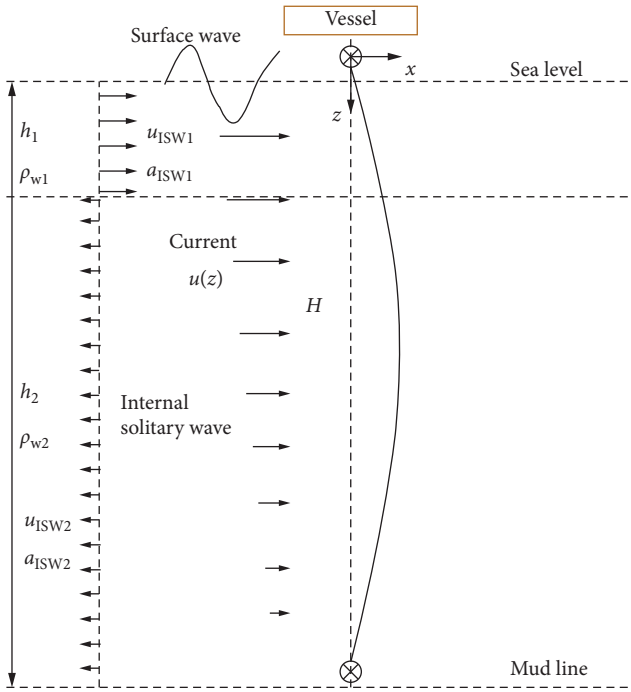

FIGURE 1: Schematic model of the marine drilling riser.

risers. Fan et al. [23] studied the dynamic response of a hang-off drilling riser considering the ISW and vessel's surge motion.

With a review of the previous research, these studies have provided useful guidance for engineering applications. However, so far, there are still some issues that require further investigation. (1) At present, most studies assume that the directions of the steady current and the propagation of the ISW are the same. However, there are few reports on the lateral dynamic response of real-scale marine drilling risers in different propagation directions of ISW. (2) The heave motion of the vessel will inevitably induce a dynamic change in the axial tension force of risers. The time-varying axial tension force has a great effect on the risers' lateral dynamic response. So far, however, there are no reports on the lateral dynamic response of marine drilling risers under combined excitations of the current, surface wave, ISW as well as the vessel's surge and heave motions.

Given this, a time-domain model based on finite element and Newmark-β methods is adopted in this paper to study the lateral dynamic responses of a real-scale marine drilling riser under combined excitations of the steady current, surface wave, ISW as well as, the vessel's surge and heave motions. The impact level of each factor in the riser's lateral dynamic response is discussed.

2. Mechanical Models

The top end of the marine drilling riser is connected to the tensioner system and can move laterally with the vessel's surge motion. The bottom end of the riser is connected to the flex joint. A pinned–pinned tensioned Euler–Bernoulli beam model is used to simulate the riser. Figure 1 shows the mechanical model of the riser. A Cartesian coordinate system is defined as follows: (1) the positive direction of the x-axis is the same as that of the steady current; (2) the z-axis is positive downward; (3) the coordinate origin is located at the top end of the undeformed vertical riser.

Considering an extreme situation, it is assumed that the lateral motion of the riser is only in the xoz plane. So, the propagation directions of the surface wave and ISW are parallel to the x-axis. Generally, the motion of the vessel consists of six patterns: surge, sway, heave, roll, pitch, and yaw [23]. In this paper, only the impacts of the vessel's surge and heave motions are considered. The vessel's surge motion direction is parallel to the x-axis, and the vessel's heave motion direction is parallel to the z-axis. The deformation of the riser is featured by a large displacement but a small strain, so the geometric nonlinearity is not considered in the present study. The rotation inertial term of the riser is also neglected. The lateral dynamic response governing equation of the riser can be written as follows [19, 24]:

$$\mathrm{EI}\frac{\partial^4 x(z,t)}{\partial z^4} - \frac{\partial}{\partial z}\left(T(z,t)\frac{\partial x(z,t)}{\partial z}\right) + \overline{m}\frac{\partial^2 x(z,t)}{\partial t^2} + c\frac{\partial x(z,t)}{\partial t} = f(z,t), \tag{1}$$

where $x(z,t)$ is the lateral displacement; t is the time; EI is the bending stiffness; $T(z,t)$ is the time-varying axial tension force; $\overline{m}$ is the equivalent mass; c is the structural damping coefficient; $f(z,t)$ is the lateral hydrodynamic force.

The time-varying axial tension force of the riser is related to the top tension force and surface wave, it can be expressed as follows [19, 20]:

$$T(z,t) = T_{\mathrm{top}} - w(H-z) + K\sum_{n=1}^{N} A_n \sin\left(k_n A_n - \omega_n t + \phi_n + \alpha_n\right), \tag{2}$$

where T_{top} is the top tension force ($T_{\mathrm{top}} = f_{\mathrm{top}} wH$); f_{top} is the top tension force coefficient; w is the wet weight per unit length of the riser; H is the water depth; K is the equivalent spring stiffness of the heave compensator ($K = wH/A_{\mathrm{c}}$); A_{c} is the critical amplitude associated with the heave compensator (usually set as 10 m); A_n is the amplitude of the vessel's heave motion; k_n, ω_n, and ϕ_n are the wave number, angular frequency, and phase angle of the random surface wave, respectively; α_n is the difference of the phase angle between the vessel's heave motion and surface wave.

The formulas of the wet weight and the corresponding mass are as follows [24]:

$$w = (m_{\mathrm{r}} + m_{\mathrm{f}} - m_{\mathrm{d}})g;\ \overline{m} = m_{\mathrm{r}} + m_{\mathrm{f}}$$
$$m_{\mathrm{r}} = \pi\rho_{\mathrm{r}}(D^2 - d^2)/4;\ m_{\mathrm{f}} = \pi\rho_{\mathrm{f}} d^2/4;\ m_{\mathrm{d}} = \pi\rho_{\mathrm{w}} D^2/4, \tag{3}$$

where m_{r}, m_{f}, and m_{d} are the masses of a unit length riser, the internal fluid of a unit length riser, and the external

discharged seawater of a unit length riser, respectively; g is the gravitational acceleration; ρ_r, ρ_f, and ρ_w are the densities of the riser, internal fluid, and external seawater, respectively; D and d are the outer and inner diameters of the riser, respectively.

The lateral hydrodynamic force acting on a unit length riser can be calculated by the modified Morison formula [19, 23]:

$$f(z,t) = 0.5C_D\rho_w D\left(u(z,t) - \frac{\partial x(z,t)}{\partial t}\right)\left|u(z,t) - \frac{\partial x(z,t)}{\partial t}\right| + \rho_w\frac{\pi D^2}{4}\left(C_M a_w(z,t) - C_a\frac{\partial^2 x(z,t)}{\partial t^2}\right), \tag{4}$$

where C_D is the drag force coefficient; C_M is the inertia force coefficient; C_a is the added mass coefficient; $u(z,t)$ and $a_w(z,t)$ are the lateral velocity and acceleration of the seawater, respectively; $\partial x(z,t)/\partial t$ and $\partial^2 x(z,t)/\partial t^2$ are the lateral velocity and acceleration of the riser, respectively.

The lateral velocity and acceleration of the seawater can be calculated as follows:

$$\begin{aligned} u(z,t) &= u_c(z) + u_{SW}(z,t) + u_{ISW}(z,t) \\ a_w(z,t) &= a_{SW}(z,t) + a_{ISW}(z,t), \end{aligned} \tag{5}$$

where $u_c(z)$, $u_{SW}(z,t)$, and $u_{ISW}(z,t)$ are the lateral velocities of the seawater induced by the steady current, surface wave, and ISW, respectively; $a_{SW}(z,t)$ and $a_{ISW}(z,t)$ are the lateral accelerations of the seawater induced by the surface wave and ISW, respectively.

The lateral velocity of the seawater induced by the steady current can be calculated with the equation recommended by the American Bureau of Shipping [25]:

$$u_c(z) = u_m((H-z)/H) + u_T((H-z)/H)^{1/7}, \tag{6}$$

where u_m and u_T are the lateral velocities of the surface seawater induced by the wind and tide, respectively.

The lateral velocity and acceleration of the seawater induced by the surface wave can be written as follows [19]:

$$\begin{aligned} u_{SW}(x,z,t) &= \sum_{n=1}^{N}\frac{gh_n k_n}{2\omega_n}\frac{\cosh k_n(H-z)}{\cosh k_n H}\cos(k_n x - \omega_n t + \phi_n) \\ a_{SW}(x,z,t) &= \sum_{n=1}^{N}\frac{gh_n k_n}{2}\frac{\cosh k_n(H-z)}{\cosh k_n H}\sin(k_n x - \omega_n t + \phi_n), \end{aligned} \tag{7}$$

where h_n is the height of a single wave.

The relationship between the wave number and angular frequency is [19]:

$$\omega_n^2 = gk_n\tanh(k_n H). \tag{8}$$

A two-layer fluid model is used to simulate the ISW. The KdV equation is adopted in this paper to simulate the ISW. The lateral velocity and acceleration of the seawater induced by the ISW are [23]:

$$u_{ISW}(x,t) = \begin{cases} \dfrac{c\eta_0}{h_1}\operatorname{sech}^2\phi & \text{in upper layer} \\ -\dfrac{c\eta_0}{h_2}\operatorname{sech}^2\phi & \text{in lower layer} \end{cases}, \tag{9}$$

$$a_{ISW}(x,z,t) = \begin{cases} \dfrac{2c\eta_0 C_p z}{h_1 l}\operatorname{sech}^2\phi\tanh\phi & \text{in upper layer} \\ -\dfrac{2c\eta_0 C_p (H-z)}{h_2 l}\operatorname{sech}^2\phi\tanh\phi & \text{in lower layer} \end{cases}, \tag{10}$$

where η_0 is the wave amplitude; h_1 and h_2 are the water thicknesses in the upper and lower layers, respectively; ρ_{w1} and ρ_{w2} are the water densities in the upper and lower layers.

$$\begin{aligned} &\phi = \left(\frac{x - C_p t}{l}\right),\ c = \sqrt{\frac{g\Delta\rho_w h_1 h_2}{\overline{\rho}_w(h_1+h_2)}}, \\ &\Delta\rho_w = \rho_{w2} - \rho_{w1},\ \overline{\rho}_w = \frac{\rho_{w1}+\rho_{w2}}{2}, \\ &C_p = c\left[1 + \frac{\eta_0(h_2-h_1)}{2h_1 h_2}\right],\ l = \frac{2h_1 h_2}{\sqrt{3\eta_0|h_2-h_1|}}. \end{aligned} \tag{11}$$

The lateral surge motion of the vessel can be expressed as follows [19, 21]:

$$\begin{aligned} S(t) = {} & S_0 + S_L\sin\left(\frac{2\pi t}{T_L} - \alpha_L\right) \\ & + \sum_{n=1}^{N} S_n\sin(k_n S(t) - \omega_n t + \phi_n + \alpha_n), \end{aligned} \tag{12}$$

where S_0 is the vessel's average offset displacement from the wellbore; S_L and T_L are the amplitude and period of the vessel's drift, respectively; α_L is the phase angle difference of the vessel's drift and surface wave (usually takes a value of zero); S_n is the amplitude of the vessel's surge motion.

The vertical fluctuation displacement of the riser's top end is usually very small due to the buffering effect of the heave compensator system. Hence, the boundary conditions can be expressed as follows:

$$x(0,t) = S(t), x(H,t) = 0, \frac{\partial^2 x(0,t)}{\partial z^2} = 0, \frac{\partial^2 x(H,t)}{\partial z^2} = 0. \tag{13}$$

According to Guo et al. [21] and Fan et al. [23], the values of the empirical coefficients in the modified Morrison formula are as follows: the drag force coefficient is 1.2, the inertia force coefficient is 2.0, and the added mass coefficient is 1.0.

Table 1: The main physical and geometric parameters of the riser model [27].

Parameters	Values	Parameters	Values
Riser length (m)	500	Young's modulus (Pa)	2.1×10^{11}
Riser outer diameter (m)	0.8120	Poisson's ratio	0.3
Riser inner diameter (m)	0.7568	Internal fluid density (kg/m^3)	850
Riser density (kg/m^3)	7,850	Top tension force (N)	3×10^5

Table 2: The parameters of the ISW [27].

Parameters	Values	Parameters	Values
Total water depth (m)	472	Upper layer water density (kg/m^3)	1,025
Upper layer water thickness (m)	60	Lower layer water density (kg/m^3)	1,028
Lower layer water thickness (m)	412	Wave amplitude (m)	75

3. Numerical Solution Methods and Program Verification

The coupling form of Equations (1–(13) is complex nonlinear partial differential equations. In order to solve the problem, the Galerkin-type finite element and Newmark-β methods are adopted in this paper. Based on the parameters of the riser and seawater as well as the boundary conditions, Hermite cubic interpolation functions are used to obtain the structural bending stiffness matrix, geometric stiffness matrix, and mass matrix. Because of the uncertainty of the structural damping coefficient, the Rayleigh damping theory is adopted in this paper to obtain the structural damping matrix. According to the parameters of the steady current, surface wave, ISW as well as, the initial and boundary conditions, the equivalent force vector can also be obtained at the initial moment. Then, the Newmark-β method is adopted to analyze the dynamic response in the time domain. The entire numerical calculation process is realized by a self-developed program based on MATLAB [26].

It is very difficult to test the combined effect of the steady current, surface wave, ISW, and vessel's motion on the marine drilling risers. Hence, so far, no relevant marine and laboratory testing results for reference. Therefore, the reliability of the numerical calculation program established in this paper is verified by comparing it with published numerical results [27]. The main physical and geometric parameters of the riser model are given in Table 1. The parameters of the ISW are given in Table 2.

The velocity profile of the nonuniform steady current used in the present study is shown in Figure 2.

According to the elemental precision analysis, the riser model is divided equally into 125 elements. The interval time is 1.0 s, and the total calculation time is 2,500 s. At the initial moment, the velocity of the riser is zero. Figure 3 shows the comparisons of the dynamic responses of the riser. The variable alpha herein denotes the angle between the steady current and the propagation direction of the ISW. It can be seen that the displacement obtained in this paper is slightly larger than that obtained by Jiang. Overall, the time-varying features of the displacement are consistent. Therefore, the numerical calculation program established in this paper can be used to study the lateral dynamic response of the marine drilling risers.

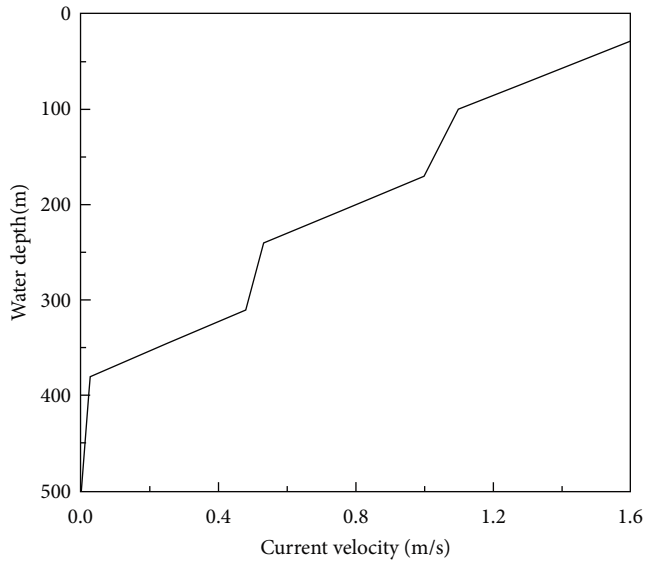

Figure 2: Velocity profile of the nonuniform steady current [27].

4. Case Study, Results, and Discussion

According to the conditions in the operation areas, the lateral velocities of the surface seawater induced by the wind and tide are all taken as 0.5 m/s. So, the seawater velocity distribution of the steady current along the water depth can be calculated using Equation (6). The velocity induced by the steady current varies only with the water depth and does not change over time.

In this paper, a deterministic effective regular wave is used to simulate the irregular random surface waves in the operation areas. A two-parameter P–M spectrum is adopted in the simulation process [28]. According to the observation data, the parameters of the deterministic effective regular surface wave and vessel's motion are given in Table 3. According to Equation (7), the velocity and acceleration

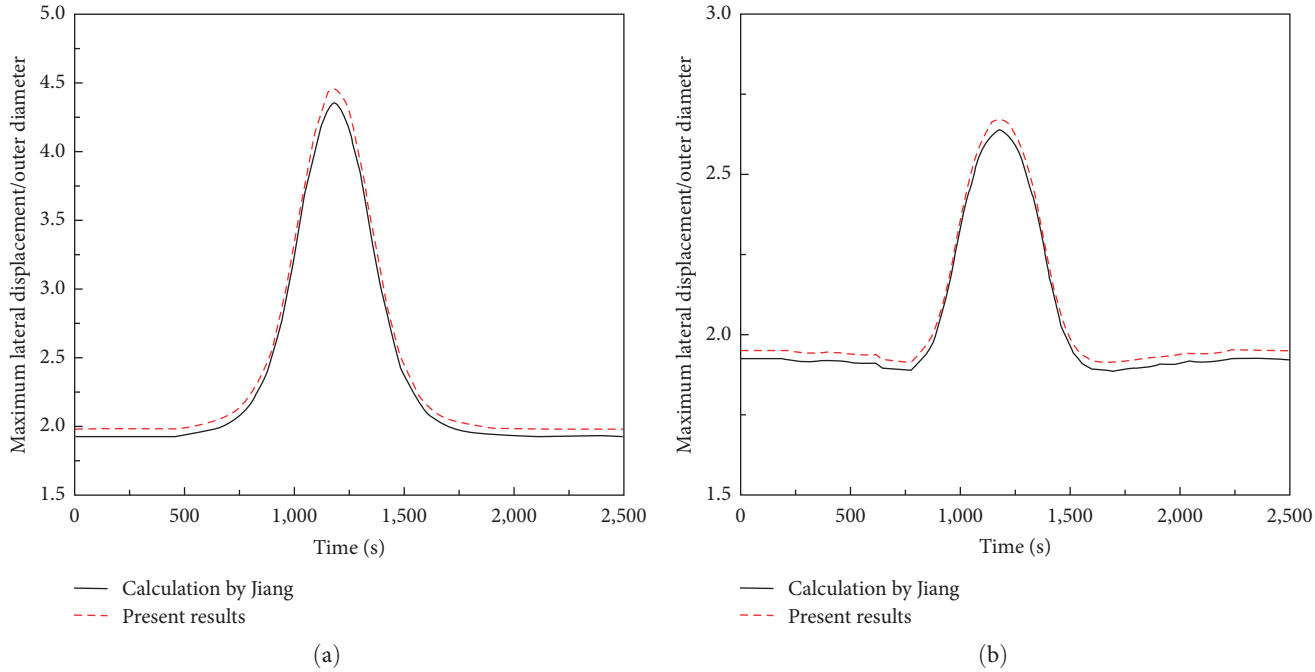

Figure 3: Comparisons of the dynamic responses of the riser [27]: (a) $\alpha = 0$ and (b) $\alpha = \pi$.

Table 3: Parameters of the effective regular surface wave and vessel motion.

Parameters	Values
Effective wave height (m)	10
Effective wave period (s)	5
Vessel's average offset displacement (m)	40
Vessel's drift amplitude (m)	10
Vessel's drift period (s)	100
Vessel's surge wave motion amplitude (m)	4
Vessel's heave wave motion amplitude (m)	2
Wave phase angle (rad)	0
Phase angle difference (rad)	0

induced by the surface wave not only change with the water depth, but they also vary over time.

The parameters of the ISW are given in Table 4. According to the conditions in the operation areas, the entire duration time of the ISW is 3,350 s. According to Equation (9), the velocities induced by the ISW in the upper and lower layers remain constant at each water depth, but they are in opposite directions. According to Equation (10), the accelerations induced by the ISW in the upper and lower layers not only change with the water depth, but they are also in the opposite directions. Meanwhile, the velocity and acceleration induced by the ISW in the upper and lower layers all change over time.

Figure 4(a) shows the distribution of the maximum seawater velocity along the water depth. The maximum velocity expressed herein refers to the maximum value of the velocity induced by the SC/ISW during the entire computing time. Figure 4(b) shows the time-varying features of the velocities of the seawater induced by the ISW in the upper and lower layers.

To facilitate descriptions, some abbreviated forms are given in Table 5.

The parameters of the marine drilling riser are given in Table 6.

According to the elemental precision analysis, the riser is divided equally into 200 elements, and the interval time is 0.1 s. At the initial moment, the velocity of the riser is zero, and the riser's centerline is at the peak position of the effective regular surface wave. The lateral dynamic responses of the riser in four different cases are analyzed in the present study. The loads of these cases are listed in Table 7.

Figure 5 shows the lateral displacement along the riser's length at different moments in Case 1 (T is the duration time of the ISW). T/2 indicates that the trough of the ISW reaches the riser's centerline, and at this moment, the velocity and acceleration of the seawater induced by the ISW reach the maximum value.

It can be seen from Figure 5(a) that the time-varying features of the displacement at different sections of the riser are different. This is due to the time-varying features of the velocity and acceleration at different water depths are different. It can be noted from Figure 5(b) that the displacement increases gradually over time.

Figure 6 displays the time history of the lateral displacement when the propagation directions of the SC and ISW are the same. It can be noted from Figure 6(a) that the fluctuation of the displacement is composed of a low frequency with a large amplitude and a high frequency with a small amplitude. The low frequency with a large amplitude fluctuation is mainly induced by the SC and ISW, while the high frequency

Table 4: The parameters of the ISW.

Parameters	Values	Parameters	Values
Total water depth (m)	2,000	Upper layer water density (kg/m^3)	1,025
Upper layer water thickness (m)	300	Lower layer water density (kg/m^3)	1,028
Lower layer water thickness (m)	1,700	Wave amplitude (m)	190

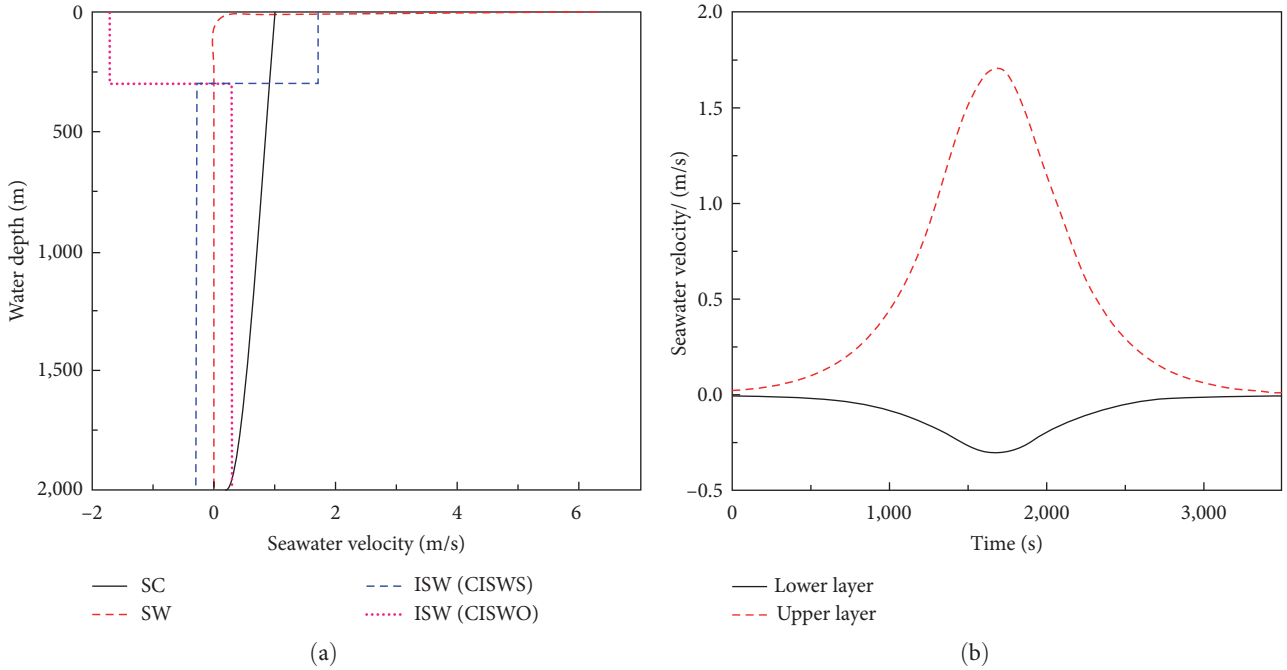

Figure 4: Distributions of the velocity of the seawater: (a) SC/SW/ISW and (b) ISW.

Table 5: Definitions of the abbreviations.

Abbreviated form	Full form
SC	Steady current
SW	Surface wave
ISW	Internal solitary wave
VS	Vessel's surge motion
VH	Vessel's heave motion
CISWS	Directions of the steady current and the propagation of the internal solitary wave are the same
CISWO	Directions of the steady current and the propagation of the internal solitary wave are opposite

with a small amplitude fluctuation is mainly induced by the SW. The magnitude of the displacement induced by the SW is much smaller than that induced by the SC and ISW. It can be seen from Figures 6(a) and 6(b) that the VS greatly changes the fluctuation amplitude and frequency of the displacement. Moreover, the impact of the VS on different sections of the riser is different. The fluctuation amplitude and frequency of the lateral displacement are mainly induced by the SC, ISW, and VS. Similarly, it can be seen from Figures 6(a) and 6(c) that the VH changes the fluctuation amplitude and frequency of the displacement. The VH mainly affects the high-frequency component of the displacement, and the impact of the VH on different sections of the riser is also different. In this situation, the low-frequency fluctuation amplitude and frequency of the displacement are mainly induced by the SC and ISW, while the high-frequency fluctuation amplitude and frequency of the displacement are mainly induced by the VH. As is shown in Figure 6(d), the fluctuation amplitude and frequency of the displacement in the lower layer all changed when the vessel's surge and heave motions are all considered. In this situation, variations of the fluctuation amplitude and frequency of the displacement in the upper layer are small. At this time, the fluctuation amplitude and frequency of the displacement are mainly induced by the SC, SW, ISW, VS, and VH.

Figure 7 shows the time history of the lateral displacement when the propagation directions of the SC and ISW are opposite. The maximum displacement and the corresponding water depth in different cases are given in Table 8.

Figure 8 presents the bending moment along the riser's length at different moments in Case 1. It can be seen from Figure 8(a) that the bending moment in the upper layer increases rapidly with time, but it decreases slowly with time in the lower layer. Because of the impact of the ISW, the bending moment changes abruptly at the interface

Table 6: The main parameters of the marine drilling riser.

Parameters	Values	Parameters	Values
Riser length (m)	2,000	Young's modulus (Pa)	2.1×10^{11}
Riser outer diameter (m)	0.5334	Poisson's ratio	0.3
Riser inner diameter (m)	0.4826	Internal fluid density (kg/m^3)	1,200
Riser density (kg/m^3)	7,850	Top tension force coefficient	1.4

Table 7: Loads of different cases.

Case	1	2	3	4
Loads	SC + SW + ISW	SC + SW + ISW + VS	SC + SW + ISW + VH	SC + SW + ISW + VS + VH

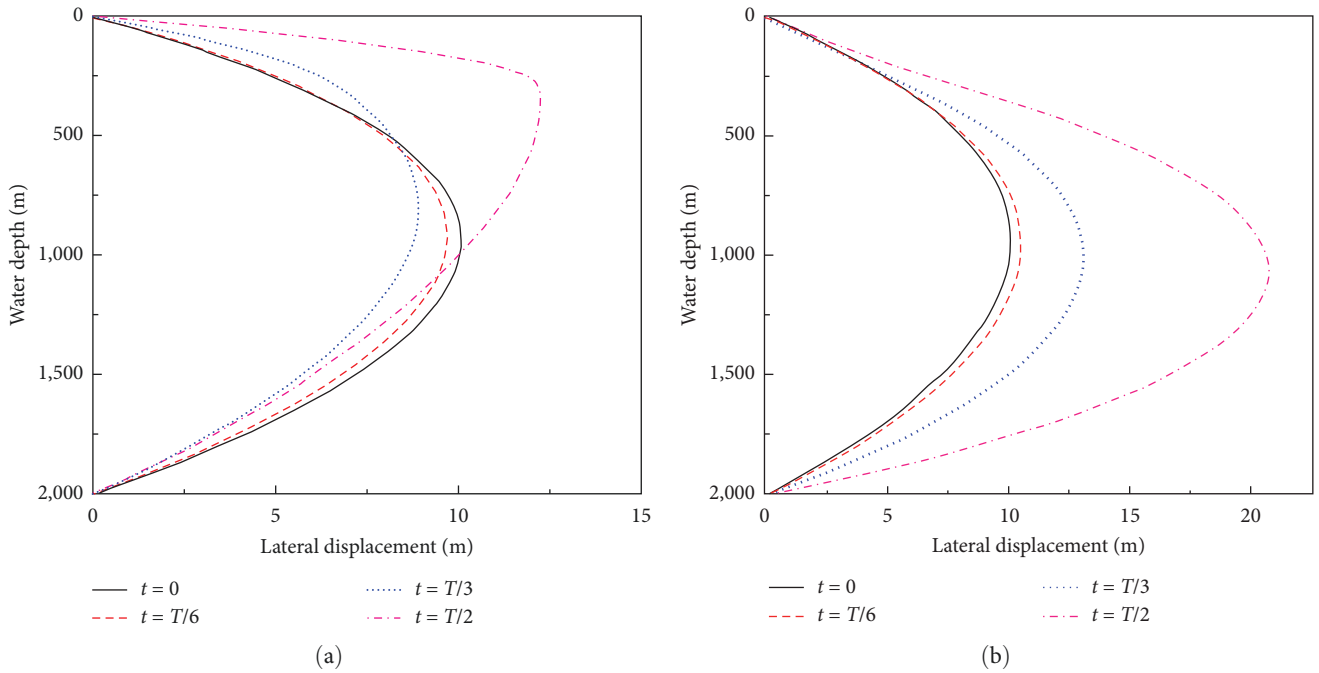

Figure 5: Lateral displacement along the riser's length at different moments: (a) CISWS and (b) CISWO.

between the upper and lower layers. This is due to the sudden change of the magnitude and direction of the seawater velocity and acceleration induced by the ISW at this location, and the riser herein is subjected to a large shear force. It can be noted from Figure 8(b) that the bending moment in the upper layer first decreases rapidly and then increases rapidly with time, but the bending moment in the lower layer increases rapidly with time.

Figure 9 displays the time history of the bending moment when the propagation directions of the SC and ISW are the same. It can be noted from Figure 9(a) that the proportion of the bending moment induced by the SW in the total bending moment is very small. The bending moment is mainly induced by the SC and ISW. It can be seen from Figures 9(a) and 9(b) that the VS changes the fluctuation amplitude and frequency of the bending moment. The VS mainly affects the high-frequency component of the bending moment, and the impact in different sections of the riser is different. The maximum fluctuation amplitude of the bending moment is mainly induced by the SC and ISW. It can be seen from Figure 9(a)–9(c) that the effects of the VS and VH on the bending moment are similar. The fluctuation amplitude of the bending moment induced by the VH is less than that induced by the VS. The fluctuation frequency of the bending moment induced by the VH is different from that induced by the VS. As is shown in Figure 9(d), the amplitude and frequency of the low-frequency fluctuation of the bending moment are mainly induced by the SC and ISW, while the amplitude and frequency of the high-frequency fluctuation of the bending moment are mainly induced by the VS and VH.

Figure 10 shows the time history of the bending moment when the propagation directions of the SC and ISW are opposite. The maximum bending moment and

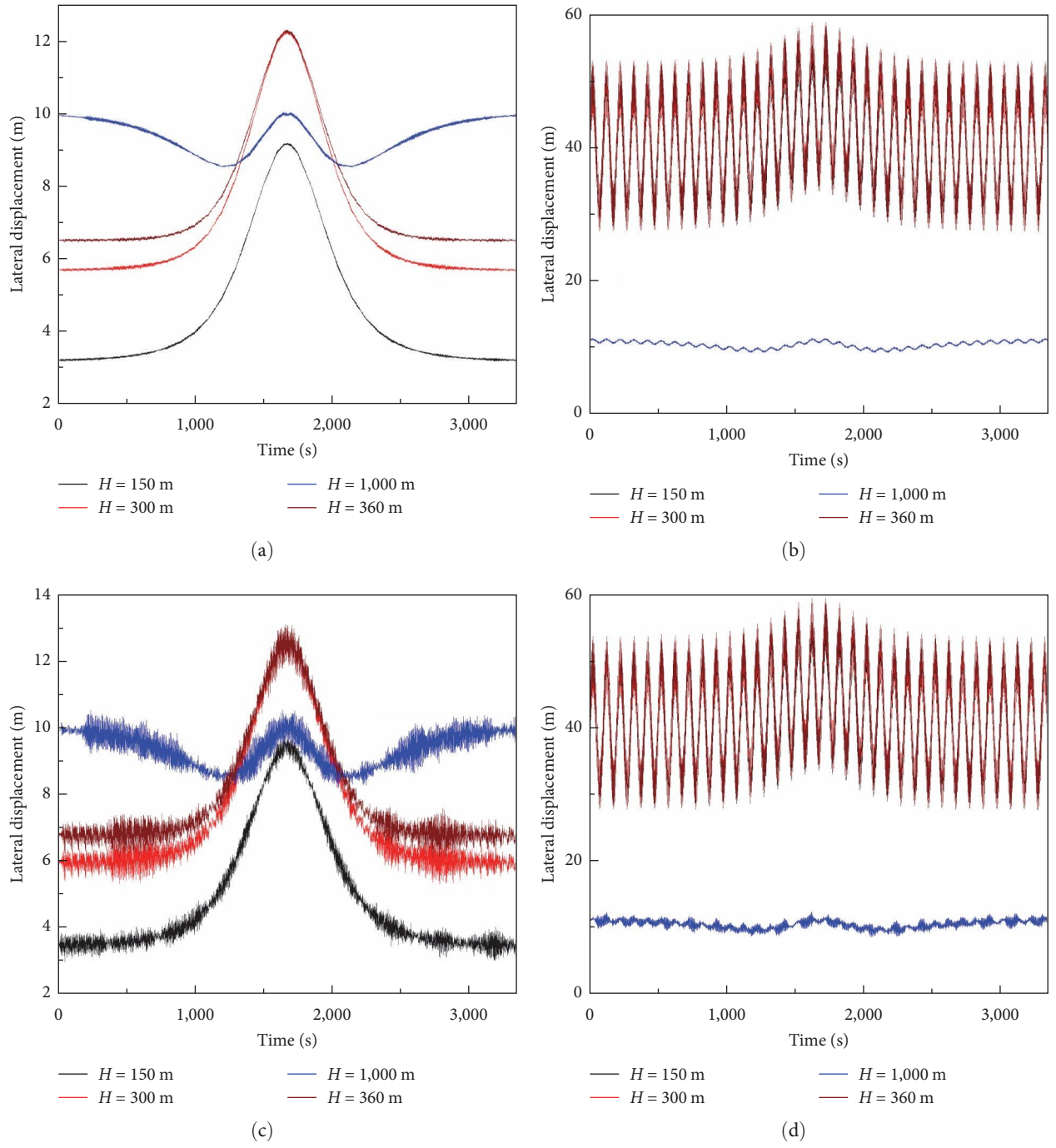

Figure 6: Time history of the riser's lateral displacement under different combined loads (CISWS): (a) SC + SW + ISW, (b) SC + SW + ISW + VS, (c) SC + SW + ISW + VH, and (d) SC + SW + ISW + VS + VH.

the corresponding water depth in different cases are given in Table 9.

According to the characteristics of the ISW, the flow direction of the upper and lower layers of the seawater caused by the ISW is opposite. When the propagation direction of the ISW is the same as the direction of the SC, the seawater flow velocity in the upper layer increases, and the seawater flow velocity in the lower layer decreases. And the seawater flow direction near the seabed changes, which is opposite to the direction of the SC. When the propagation direction of the ISW is opposite to the direction of the SC, the seawater flow velocity in the upper layer decreases, and at this time, the seawater flow direction is opposite to the direction of the SC. At this time, the seawater flow velocity in the lower layer increases. Moreover, due to the periodic changes in seawater flow velocity caused by the ISW, the magnitude, direction, and frequency of changes in the seawater flow velocity vary at different depths of water. The specific changes can be

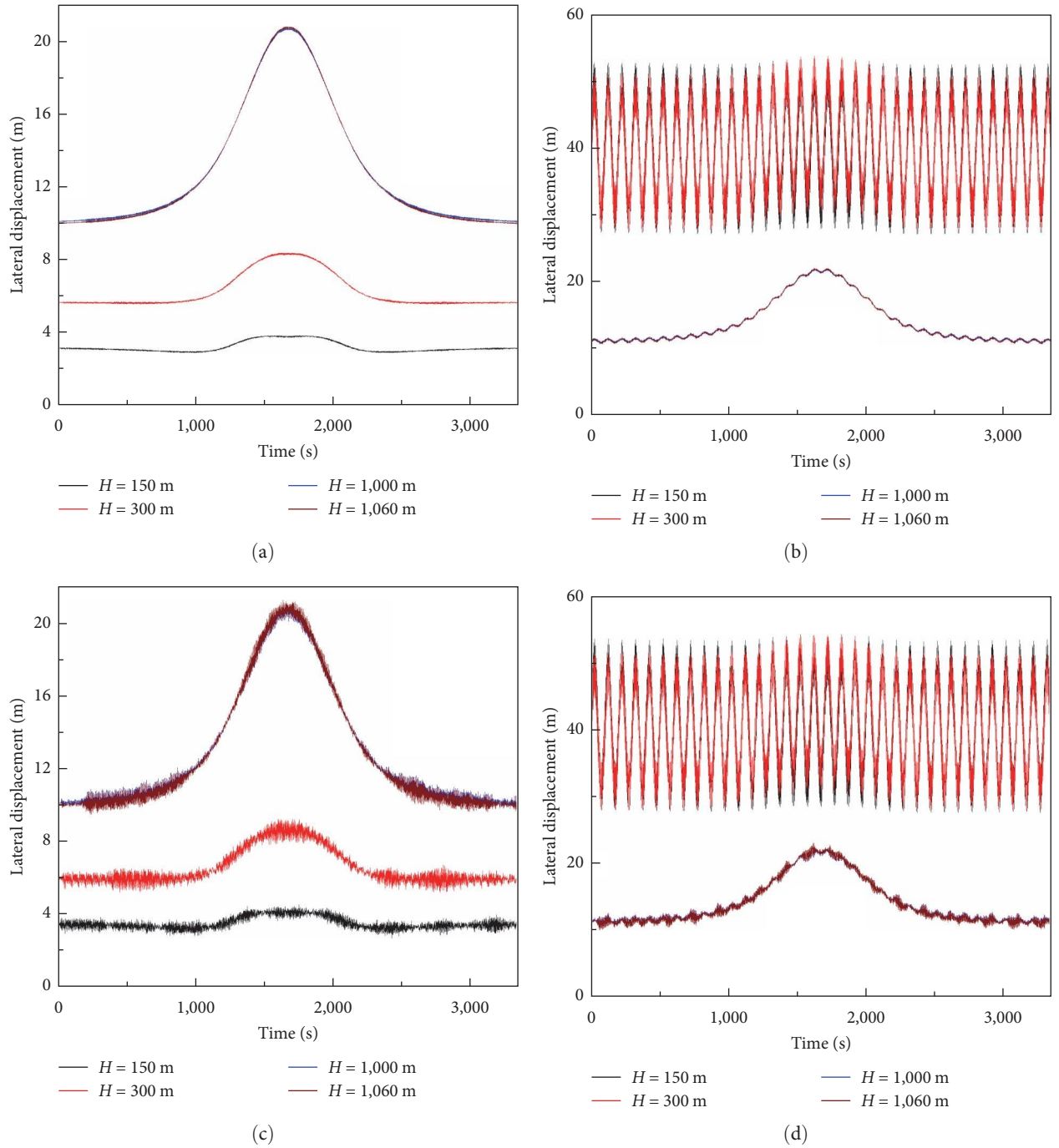

Figure 7: Time history of the riser's lateral displacement under different combined loads (CISWO): (a) SC + SW + ISW, (b) SC + SW + ISW + VS, (c) SC + SW + ISW + VH, and (d) SC + SW + ISW + VS + VH.

Table 8: Maximum lateral displacement and corresponding water depth in different cases.

	Case							
	CISWS				CISWO			
	1	2	3	4	1	2	3	4
Displacement (m)	12.23	56.45	13.1	56.58	20.73	53.96	21.27	54.26
Water depth (m)	360	360	360	360	1,060	300	1,060	300

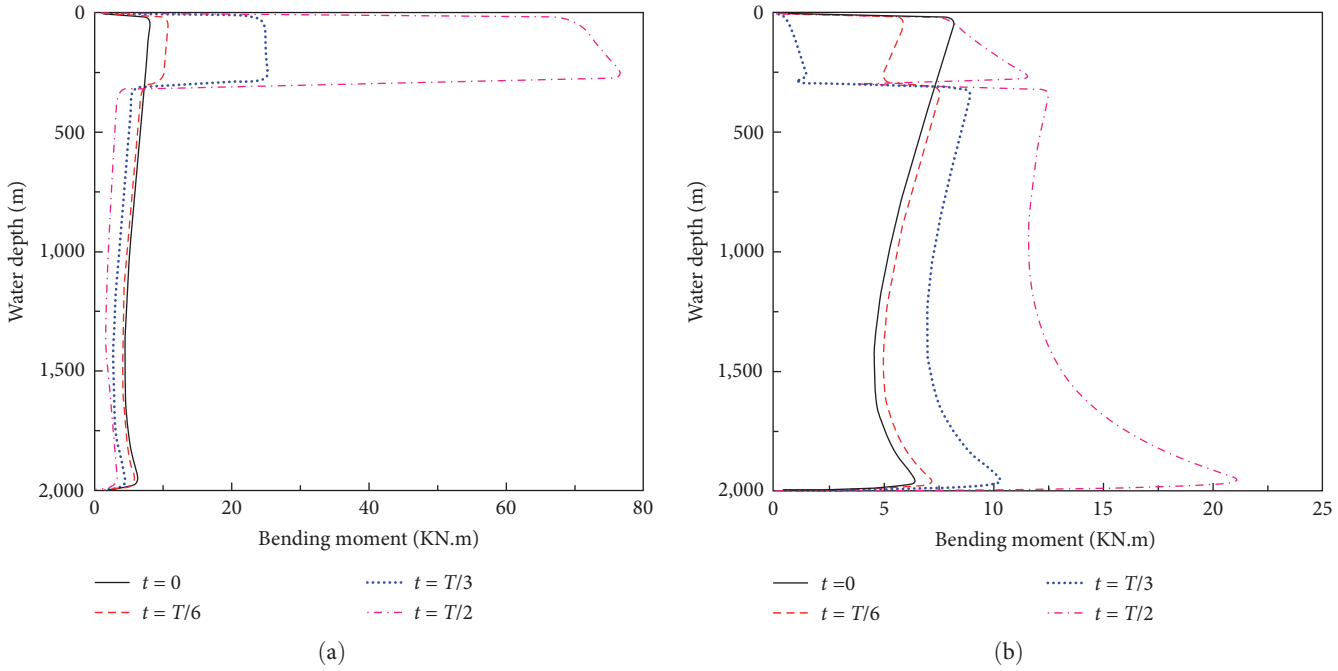

FIGURE 8: Bending moment along the riser's length at different moments: (a) CISWS and (b) CISWO.

obtained from Equations (6), (7), and (9) and Figure 4. Similarly, the variation patterns of the seawater flow acceleration at different water depths can be obtained from Equations (7) and (9). It is precisely due to the complex changes in seawater flow that when the propagation direction of the ISW changes, the impact on the riser lateral dynamic response is also different.

Therefore, when the situation changes from CISWS to CISWO, it can be seen from Figures 5–10 to Tables 8 and 9 that the variations of the lateral displacement and bending moment mainly manifested in the following aspects:

(1) During the entire duration of the ISW, the riser maximum lateral displacement has changed. When the vessel's surge motion is not considered, the maximum lateral displacement of the riser increases. Meanwhile, the riser maximum bending moment has decreased during the entire duration of the ISW. This is because the maximum seawater flow velocity caused by the change in the propagation direction of the ISW has decreased, resulting in the changes in the maximum lateral displacement and bending moment of the riser.

(2) When the propagation direction of the ISW changes, the amplitude and direction of the seawater flow velocity and acceleration have changed at different water depths. Hence, the distributions of the riser lateral displacement and bending moment along the riser's length have changed. The positions of the maximum lateral displacement and bending moment of the riser have also changed. When the propagation direction of the ISW is the same as the SC flow direction, the maximum lateral displacement and bending moment of the riser are located at the upper part of the riser. When the propagation direction of the ISW is opposite to the SC flow direction and the vessel's surge motion is not considered, the riser maximum lateral displacement is located in the middle of the riser, while the riser maximum bending moment is located at the bottom of the riser.

(3) During the entire duration of the ISW, the time-varying features of the riser displacement and bending moment have significantly changed. Not only did the amplitude of the riser lateral displacement and bending moment fluctuations change, but the frequency of the riser lateral displacement and bending moment fluctuations also changed. And this trend of change also varies at different positions of the riser. This is because the variation characteristics of the amplitude, direction, and frequency of the seawater flow velocity and acceleration at different water depths are different, and the impact on the riser lateral dynamics is not the same, resulting in inconsistent changes in the lateral dynamic response at different positions of the riser.

(4) It is precisely because of the complex impact of changes in the propagation direction of the ISW on the seawater flow velocity and acceleration that other factors have varying degrees of influence on the riser lateral dynamic response. The proportion of displacement induced by the SC and SW in the total displacement has increased, and the proportion of displacement induced by the VS and VH in the total displacement has decreased. In addition, the proportion of the bending

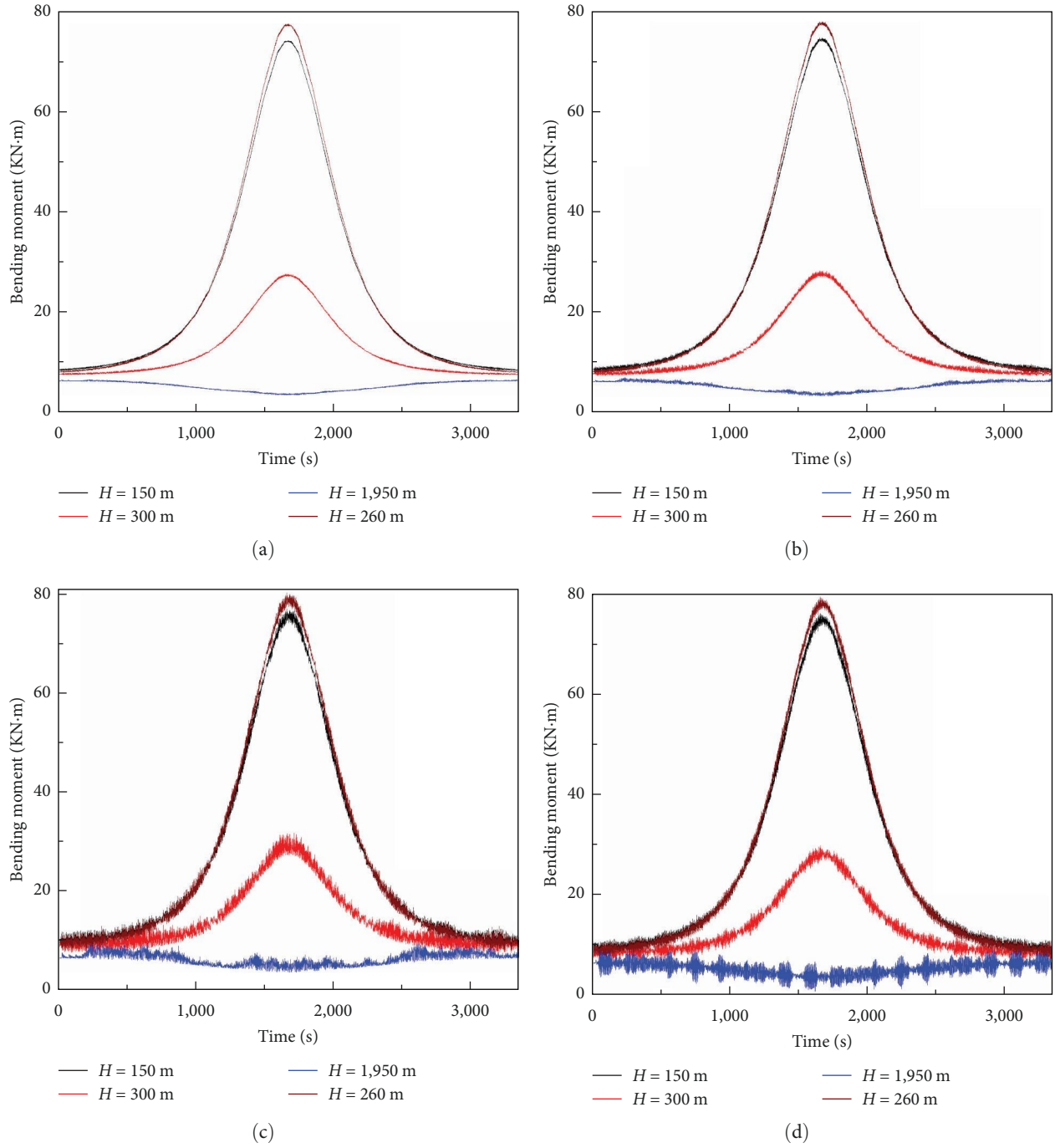

Figure 9: Time history of the riser's bending moment under different combined loads (CISWS): (a) SC + SW + ISW, (b) SC + SW + ISW + VS, (c) SC + SW + ISW + VH, and (d) SC + SW + ISW + VS + VH.

moment induced by the SW, VS, and VH in the total bending moment has increased.

As shown in the above figures, the maximum displacement and bending moment are not at the same point of the riser in both CISWS and CISWO situations. Besides, the distributions of the displacement and bending moment along the riser's length are different in the different situations. Furthermore, in different situations, the time-varying features of the displacement and bending moment are also different. And this paper only considers the two special propagation directions of the ISW. When the propagation direction of the ISW changes irregularly, the lateral dynamic response characteristics of the riser will become more complex. Therefore, this

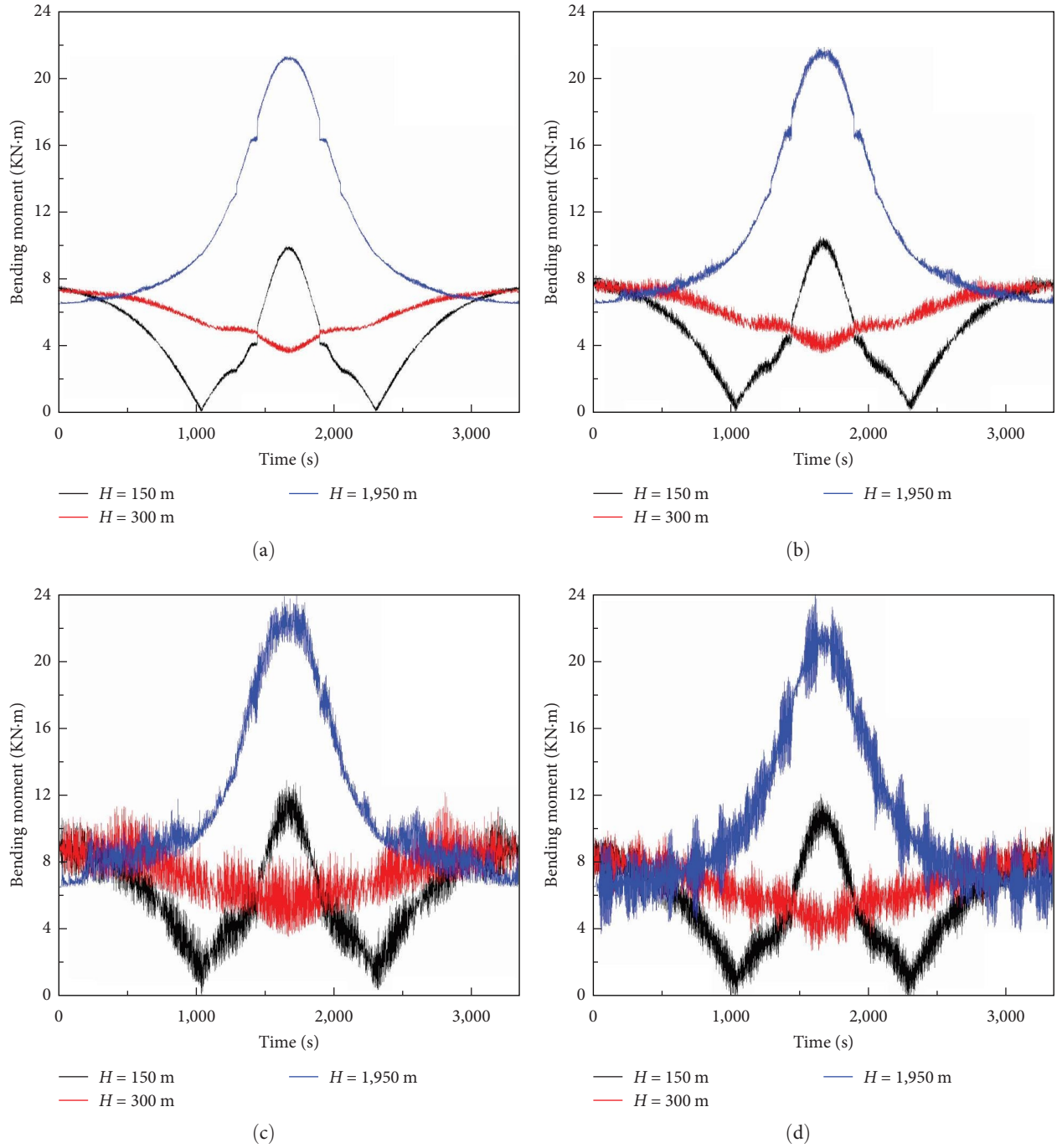

Figure 10: Time history of the riser's bending moment under different combined loads (CISWO): (a) SC + SW + ISW, (b) SC + SW + ISW + VS, (c) SC + SW + ISW + VH, and (d) SC + SW + ISW + VS + VH.

Table 9: Maximum bending moment and corresponding water depth in different cases.

	Case							
	CISWS				CISWO			
	1	2	3	4	1	2	3	4
Bending moment (KN · m)	77.15	77.94	80.28	79.46	21.1	21.83	23.9	23.96
Water depth (m)	260	260	260	260	1,950	1,950	1,950	1,950

requires full consideration in practical engineering designs of masrine drilling risers.

5. Conclusions

In this paper, the dynamic responses of a real-scale marine drilling riser under combined excitations of the steady current, surface wave, ISW as well as, the vessel's surge and heave motions are studied. Several conclusions can be drawn as follows:

(1) The vibration of the riser is a coupling form of a low frequency with a large amplitude and a high frequency with a small amplitude during the entire duration of the ISW.

(2) The low frequency with a large amplitude vibration is mainly induced by the steady current, ISW, and vessel's surge motion. The high frequency with a small amplitude vibration is mainly induced by the surface wave and vessel's heave motion.

(3) Variations in the propagation direction of the ISW will significantly change the maximum displacement and bending moment. When the propagation direction changes, the distribution of the displacement and bending moment along the riser's length will notably change, and the time-varying features of the displacement and bending moment will also notably change.

(4) The heave motion of the vessel not only significantly increases the amplitude of the riser's high-frequency vibration, but it also changes the frequency component of the riser's high-frequency vibration.

Data Availability

All data used to support the findings of this study are included in the article. The data included in this study are available upon request by contacting the corresponding author.

Conflicts of Interest

The authors declared no potential conflicts of interest with respect to the research, authorship, and/or publication of this paper.

Acknowledgments

The authors gratefully acknowledge the support from the Scientific research start up fund for college teachers (grant no. 2220017).

References

[1] S. Cai, J. Xie, and J. He, "An overview of internal solitary waves in the South China Sea," *Surveys in Geophysics*, vol. 33, pp. 927–943, 2012.

[2] R.-C. Lien, F. Henyey, B. Ma, and Y. J. Yang, "Large-amplitude internal solitary waves observed in the northern South China Sea: properties and energetics," *Journal of Physical Oceanography*, vol. 44, no. 4, pp. 1095–1115, 2014.

[3] V. D. Djordjevic and L. G. Redekopp, "The fission and disintegration of internal solitary waves moving over two-dimensional topography," *Journal of Physical Oceanography*, vol. 8, no. 6, pp. 1016–1024, 1978.

[4] K. R. Helfrich and W. Kendall Melville, "Long nonlinear internal waves," *Annual Review of Fluid Mechanics*, vol. 38, pp. 395–425, 2006.

[5] S. Cai, S. Wang, and X. Long, "A simple estimation of the force exerted by internal solitons on cylindrical piles," *Ocean Engineering*, vol. 33, no. 7, pp. 974–980, 2006.

[6] S. Cai, X. Long, and S. Wang, "Forces and torques exerted by internal solitons in shear flows on cylindrical piles," *Applied Ocean Research*, vol. 30, no. 1, pp. 72–77, 2008.

[7] J. Xie, J. Xu, and S. Cai, "A numerical study of the load on cylindrical piles exerted by internal solitary waves," *Journal of Fluids and Structures*, vol. 27, no. 8, pp. 1252–1261, 2011.

[8] Z. Si, Y. Zhang, and Z. Fan, "A numerical simulation of shear forces and torques exerted by large-amplitude internal solitary waves on a rigid pile in South China Sea," *Applied Ocean Research*, vol. 37, pp. 127–132, 2012.

[9] Z. Xu, B. Yin, H. Yang, and J. Qi, "Depression and elevation internal solitary waves in a two-layer fluid and their forces on cylindrical piles," *Chinese Journal of Oceanology and Limnology*, vol. 30, pp. 703–712, 2012.

[10] G. Zha, Y. He, T. Yu, Q. He, and H. Shen, "The force exerted on a cylindrical pile by ocean internal waves derived from nautical X-band radar observations and *in-situ* buoyancy frequency data," *Ocean Engineering*, vol. 41, pp. 13–20, 2012.

[11] G. Wei, H. Du, X. H. Xu et al., "Experimental investigation of the generation of large-amplitude internal solitary wave and its interaction with a submerged slender body," *Science China Physics, Mechanics and Astronomy*, vol. 57, pp. 301–310, 2014.

[12] H. Du, G. Wei, M. Gu, X. Wang, and J. Xu, "Experimental investigation of the load exerted by nonstationary internal solitary waves on a submerged slender body over a slope," *Applied Ocean Research*, vol. 59, pp. 216–223, 2016.

[13] J. Cui, S. Dong, Z. Wang, X. Han, and M. Yu, "Experimental research on internal solitary waves interacting with moored floating structures," *Marine Structures*, vol. 67, Article ID 102641, 2019.

[14] M. Chen, K. Chen, and Y.-X. You, "Experimental investigation of internal solitary wave forces on a semi-submersible," *Ocean Engineering*, vol. 141, pp. 205–214, 2017.

[15] M. Chen, K. Chen, Y.-X. You, and H.-T. Yu, "Experimental study of forces on a multi-column floating platform in internal solitary waves," *Applied Ocean Research*, vol. 78, pp. 192–200, 2018.

[16] X. Wang, J.-F. Zhou, Z. Wang, and Y.-X. You, "A numerical and experimental study of internal solitary wave loads on semi-submersible platforms," *Ocean Engineering*, vol. 150, pp. 298–308, 2018.

[17] C. S. Ye and G. G. Shen, "Numerical calculation and analysis about internal wave's force on small-scale cylinder," *Journal of Tianjin University*, vol. 38, no. 2, pp. 102–108, (In Chinese), 2005.

[18] Z. J. Song, B. Teng, Y. Gou et al., "Comparisons of internal solitary wave and surface wave actions on marine structures and their responses," *Applied Ocean Research*, vol. 33, no. 2, pp. 120–129, 2011.

[19] R. M. Sexton and L. K. Agbezuge, "Random wave and vessel motion effects on drilling riser dynamics," in *Offshore Technology Conference*, pp. 391–404, OnePetro, Houston, Texas, Paper Number: OTC-2650-MS, May 1976.

[20] H.-I. Park and D.-H. Jung, "A finite element method for dynamic analysis of long slender marine structures under combined parametric and forcing excitations," *Ocean Engineering*, vol. 29, no. 11, pp. 1313–1325, 2002.

[21] H. Guo, L. Zhang, X. Li, and M. Lou, "Dynamic responses of top tensioned riser under combined excitation of internal solitary wave, surface wave and vessel motion," *Journal of Ocean University of China*, vol. 12, pp. 6–12, 2013.

[22] I. Adamiec-Wójcik, L. Brzozowska, and Ł. Drąg, "An analysis of dynamics of risers during vessel motion by means of the rigid finite element method," *Ocean Engineering*, vol. 106, pp. 102–114, 2015.

[23] H. Fan, C. Li, Z. Wang, L. Xu, Y. Wang, and X. Feng, "Dynamic analysis of a hang-off drilling riser considering internal solitary wave and vessel motion," *Journal of Natural Gas Science and Engineering*, vol. 37, pp. 512–522, 2017.

[24] G. Gao, X. Cong, Y. Cui, and X. Qiu, "Study on vortex-induced vibration of deep-water marine drilling risers in linearly sheared flows in consideration of changing added mass," *Mathematical Problems in Engineering*, vol. 2020, Article ID 7687280, 16 pages, 2020.

[25] Y. Wang, D. Gao, and J. Fang, "Static analysis of deep-water marine riser subjected to both axial and lateral forces in its installation," *Journal of Natural Gas Science and Engineering*, vol. 19, pp. 84–90, 2014.

[26] R. Q. Xu, *Finite Element Method in Structural Analysis and MATLAB Program*, China Communications Press, China, (In Chinese), 2006.

[27] W. J. Jiang, Z. Y. Lin, Y. X. You et al., "Dynamic characteristics of a top tension riser under combined internal solitary wave and non-uniform current," *Chinese Journal of Hydrodynamics*, vol. 27, no. 4, pp. 424–435, (In Chinese), 2012.

[28] Y. J. Chang, *Design approach and its application for deepwater drilling risers*, Ph.D (Thesis), (In Chinese), China University of Petroleum (East China), 2008.